International Journal of Mass Spectrometry 223–224 (2003) 713–732

www.elsevier.com/locate/ijms

Accelerator mass spectrometry of heavy long-lived radionuclides

Christof Vockenhuber[a,*], Irshad Ahmad[b], Robin Golser[a], Walter Kutschera[a], Vitaly Liechtenstein[c], Alfred Priller[a], Peter Steier[a], Stephan Winkler[a]

[a] *Vienna Environmental Research Accelerator, Institute for Isotopic Research and Nuclear Physics, University of Vienna, A-1090 Vienna, Austria*

[b] *Physics Division, Argonne National Laboratory, Argonne, IL 60439, USA*

[c] *Russian Research Center, "Kurchatov Institute", Institute of Nuclear Fusion, 123182 Moscow, Russia*

Received 16 February 2002; accepted 29 June 2002

Abstract

This paper describes the upgrade of the Vienna Environmental Research Accelerator (VERA) to a universal facility for accelerator mass spectrometry (AMS). As a result, it is now possible to measure many long-lived radionuclides at natural abundances across the nuclear chart, from the lightest (^{10}Be) to the heaviest (^{244}Pu). Particular emphasis is placed on measurements to understand the ion optics and the origin of background ions, which ultimately limit the sensitivity. VERA is now ready to venture into the realm of actinides (e.g., ^{236}U, ^{244}Pu), and other heavy radionuclides (e.g., ^{182}Hf), which promise interesting applications in astrophysics and other fields. (Int J Mass Spectrom 223–224 (2003) 713–732)

Keywords: Accelerator mass spectrometry; Heavy radionuclides; VERA

1. Introduction

Accelerator mass spectrometry (AMS) started about 25 years ago at nuclear physics laboratories [1]. Since then, it evolved into the most versatile method to measure minute isotope ratios (10^{-10} to 10^{-16}) in small samples [2]. It now touches almost every field of the environment at large [3,4]. AMS revolutionized the use of long-lived radionuclides by detecting the radioactive atoms directly rather than their infrequent radioactive decay. In this way, one gains many orders of magnitude in detection sensitivity, reducing, e.g., sample sizes for ^{14}C dating from grams to milligrams, and the measuring times from days to hours. Some cosmogenic radionuclides (e.g., ^{41}Ca) were undetectable at natural abundances through their beta-decay, and only became available through AMS [5,6].

Almost all AMS facilities can be understood as two mass spectrometers (called "injector" and "analyzer") linked with a tandem accelerator (Fig. 1). Such a system combines the advantage of using negative ions in the injector with a stripping process to positive ions in the tandem accelerator (dissociating molecules), and the subsequent analysis of these ions on the high-energy side. Since not all elements form negative ions,

* Corresponding author.
E-mail: christof.vockenhuber@univie.ac.at

1387-3806/02/$ – see front matter
PII S1387-3806(02)00944-2

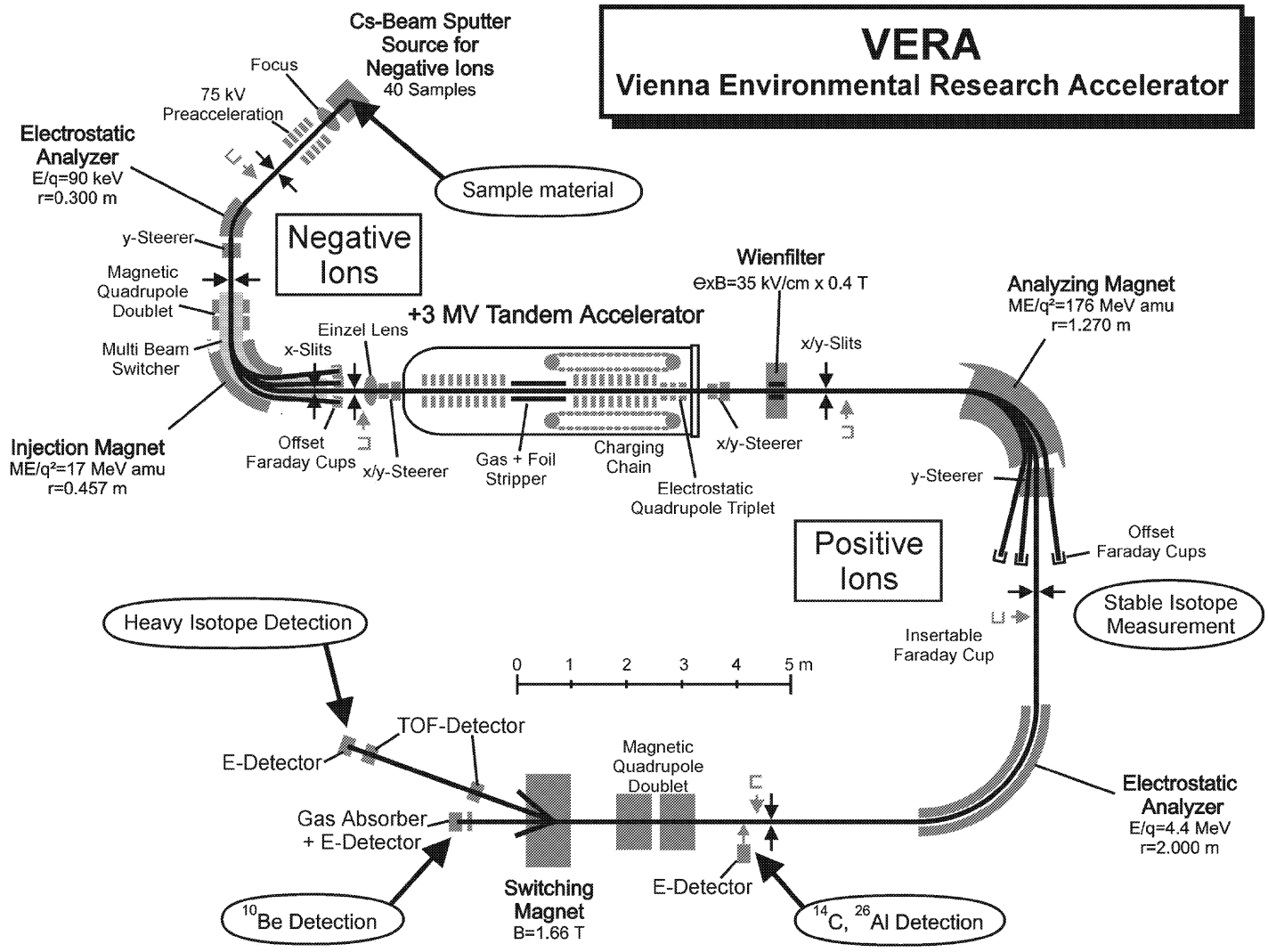

Fig. 1. Schematic layout of the VERA facility after the upgrade for heavy ions. Negative ions are used at the low-energy injection side, and positive ions at the high-energy analyzing side after stripping in the accelerator. For details see Section 2. The original layout of the facility can be found in [11].

isobaric interferences can be effectively suppressed in some important cases. For example, the detection of ^{14}C is greatly alleviated by the non-existence of $^{14}N^-$ ions [7]. It is also possible to use suitable negative molecular ions of radionuclides to suppress the interference from stable isobars. For example, the radionuclide ^{41}Ca is injected as $^{41}CaH_3^-$, which greatly suppresses ^{41}K background because $^{41}KH_3^-$ does not form stable negative ions [8]. On the other hand, the strong molecular background of $^{12}CH_2^-$ and $^{13}CH^-$ ions, which makes a detection of $^{14}C^-$ at the injector impossible, can be eliminated by dissociating the molecules in the stripping process in the tandem accelerator. Furthermore, the higher energies of the ions after acceleration allow an additional separation of the wanted ions from possible background ions at the particle detector. This method allows measurements of isotopic ratios well below 10^{-10}, where many interesting long-lived radionuclides in nature are expected (e.g., ^{10}Be, $t_{1/2} = 1.5 \times 10^6$ a; ^{14}C, 5.73×10^3 a; ^{26}Al, 7.2×10^5 a; ^{36}Cl, 3.01×10^5 a; ^{41}Ca, 1.04×10^5 a; ^{129}I, 1.6×10^7 a).

The detection of the heaviest long-lived radionuclides (e.g., ^{236}U, 2.34×10^7 a; ^{244}Pu, 8.1×10^7 a) with AMS is alleviated by the lack of stable isobars in this mass range. Therefore, it was possible to perform the first AMS detection of natural ^{236}U at a small tandem accelerator facility [9]. Larger accelerators (built for nuclear physics) have the advantage of higher energies, which helps for the separation and identification of the radionuclides from interfering background [10], especially if stable isobar separation is needed. The relative mass difference between the radionuclides of interest and its neighboring isotopes generally becomes smaller for higher masses, so both the injector and the analyzer must provide sufficient resolution. At lower energies with small tandem accelerators all components must be well designed to achieve the desired reduction of interfering background. Small machines can offset this disadvantages of lower energy by higher flexibility and stability. Moreover, in cases where no negative ions of the interfering stable isobars exist, an even better sensitivity can be achieved with lower effort. The necessary modifications of the VERA AMS system from the original setup [11] and our first experiences with heavy isotope AMS will be presented.

2. The VERA AMS system

The AMS facility at the University of Vienna, the Vienna Environmental Research Accelerator (VERA), is based on an AMS system with a 3-MV Pelletron tandem accelerator, built by National Electrostatics Corporation (NEC) in Wisconsin, USA. Despite the modest terminal voltage of 3 MV, one goal of the VERA facility has always been to extend AMS measurements across the whole nuclear chart. Therefore, the main components of the original machine [11] allow the transport of all ions from the lightest to the heaviest. To achieve the ultimate sensitivity and stability, all components are designed to avoid beam losses. High selectivity is not obtained by a single component with extremely high resolution, but by several elements with lower resolution and high transmission.

Since the installation of VERA in 1996, we have extended the measuring capabilities of the original system considerably. The schematic layout of the new setup is shown in Fig. 1. In the following, we briefly describe the main elements of the system.

2.1. The ion source

The ion source is of the so-called Multi-Cathode Source for Negative Ions by Cesium Sputtering type (MC-SNICS) [12]. The source contains a target wheel holding up to 40 pre-treated, solid samples of typically a few mg material and 1 mm diameter. Under normal running conditions, each sample can be sputtered with the cesium beam for several hours. Only the resulting negative ions (e.g., $<10\%$ of all sputtered ions for carbon) can be used. The fraction of negative ions varies appreciably for different elements, and can actually be well below 1% for elements with low electron affinities. For chemical elements which do not form negative atomic ions well (e.g., alkaline earth elements), negative molecular ions can be used. In some cases, a proper choice of the negative ion species also

allows one to suppress stable isobars (see Section 6.4). On the other hand, an unsuitable sample material or a disadvantageous choice of the ion species will compromise the effectiveness of the injector mass spectrometer if interfering molecular isobars exist. Hydrides can often cause problems since different isotopes of the same element can be simultaneously injected with different numbers of hydrogen atoms. Oxides usually show reasonable yields of negative ions (we observe up to 100 nA for $^{238}U^{16}O^-$). However, for the detection of the rare isotope of uranium, ^{236}U, the $^{236}U^{16}O^-$ ions will be accompanied by the more abundant $^{235}U^{17}O^-$ and $^{234}U^{18}O^-$ ions. These considerations suggest that often fluorides will be the best choice, since fluorine combines the advantages of a single stable isotope (^{19}F) with a large electron affinity of the corresponding molecules (see Section 6.1).

2.2. The low-energy injection system

The negative ions are pre-accelerated to a maximum injection energy E_{inj} of 80 keV. The energy distribution of negative ions from the Cs sputter source is narrow, but shows a small high-energy "tail" of excess energy transferred from the Cs^+ ions in the sputter process [13]. The energy selection is provided by a 45° electrostatic analyzer with a gap of 50 mm, a nominal bending radius of 300 mm and a maximum electric field strength of 6 kV/cm, resulting in an energy/charge state ratio $E_{inj}/q = 90$ keV. Its spherical electrodes provide both horizontal and vertical focusing.

With the energy fixed, a single mass M_{inj} is selected by a 90° bending magnet of 0.457 m radius and a maximum field of 1.31 T (Tesla). The maximal mass energy product ($M_{inj}\ E_{inj}/q^2$) of the injection magnet is 17 MeV amu. In the original setup its resolution was not sufficient, mainly due to astigmatic focusing. A magnetic quadrupole doublet just in front of the magnet corrected this. An additional horizontal slit was installed 40 cm closer to the injection magnet than the original slit assembly where a stigmatic beam waist can be created [14]. The maximal usable mass resolution of the injector is now $M/\Delta M \sim 900$ (see Fig. 2). For the heaviest ions (e.g., $^{244}Pu^{16}O^-$), the bending power of this magnet limits the ion energy from the source to 56 keV, which apparently does not cause any disadvantages.

To select different masses without changing the magnetic field we can vary the energy of the ions inside the injection magnet. This is achieved by applying an additional accelerating voltage of up to 13 kV to the (electrically insulated) magnet vacuum chamber. This voltage can be changed very fast (<100 μs), which allows fast sequencing of different ion species [15].

2.3. The tandem accelerator

The +3-MV tandem accelerator is of the Pelletron type (model 9SDH-2 [16]) inside a vessel filled with SF_6 at a pressure of about 6 bar. Two charging chains can supply a total charging current of about 230 μA. Resistors are used to divide the terminal voltage along the accelerator tubes.

The terminal voltage (TV) is stabilized through the current drained by a corona probe. The signal from a generating voltmeter measuring the terminal voltage is used for voltage stabilization. In this way slit stabilization (often used at accelerators for nuclear physics) was not required for stable operation. The terminal voltage can be kept constant at 3 MV with an rms deviation of ±300 V [15]. The stability of the terminal voltage is necessary to have a stable beam at the succeeding analyzer. In our case, the resolution is not limited by the small jitter of the beam.

The injected ions are accelerated by the positive high voltage towards a gas-filled channel ("stripper"), where they loose electrons and gain high positive charge states and therefore are accelerated a second time by the same potential. This results in an energy of several MeV:

$$E = (E_{inj} + e\,TV)\frac{M}{M_{inj}} + q\,e\,TV \quad (1)$$

M_{inj} is the injected mass of the (possible molecular) ion and M is the atomic mass of the ion analyzed with the charge state q.

The stripping process at the terminal has the advantage that it dissociates molecular ions, if enough

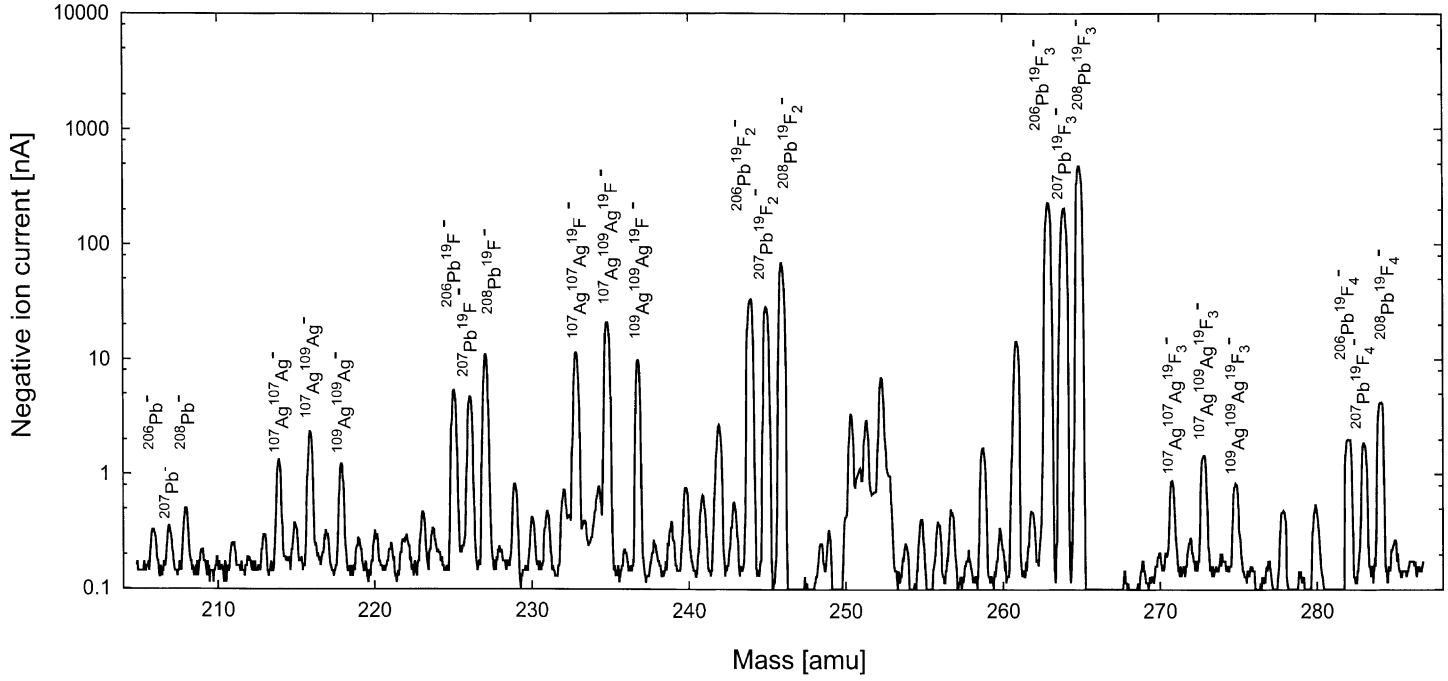

Fig. 2. Negative-ion mass spectrum from a PbF_2 target mixed with Ag powder, as measured after the injector magnet. The magnet scan shows the high mass resolution (~900) achieved with the new injector slits (object and image slits are set to approximately ± 0.5 mm). The good separation of adjacent mass peaks can be seen from the PbF_3^- ions, where the current between peaks drops by at least 3 orders of magnitude. Transmission through the slits and the accelerator is ~80%.

electrons are stripped off. The stripper canal is filled with argon gas up to a few microbar pressure, and is differentially pumped by two turbo pumps at the terminal, which re-circulate the stripper gas.

2.4. The high-energy analyzing system

By selecting a sufficiently high charge state of the wanted ions, where no molecular ions can exist, the analyzing mass spectrometer efficiently removes molecular break-up products. One main component of the analyzer is a double focusing 90° analyzing magnet with a nominal radius of 1.27 m and a maximum field of 1.53 T. The maximal ME/q^2 is 176 MeV amu. At 3 MV terminal voltage it can bend the heaviest elements with charge state 5+ or higher. As an example, Fig. 3a shows the negative ion mass spectrum from a U_3O_8 sample. Injecting $^{238}U^{16}O^-$ ions, Fig. 3b shows the various positively charged ^{16}O and ^{238}U ions separated with the analyzing magnet.

In particular, for heavy ion measurements it is important to have at least two high-resolution filter elements at the analyzer. In 2001, we replaced the low-resolution Wien-filter, which was originally installed after the analyzing magnet [14], with a new electrostatic analyzer (ESA) with the required high resolution. The ESA was built by Danfysik in Denmark, and the spherical electrodes provide both horizontal and vertical focusing. The Wien-filter was moved to a location between the exit of the tandem accelerator and the analyzing magnet (see Fig. 1) for future use as an additional analyzing component. The radius of the ESA (2.0 m), the bending angle (90°), the gap between the aluminum electrodes (45 mm), and the maximal voltage (±100 kV) result in an energy/charge state ratio of $E/q = 4.4$ MeV. The ESA was positioned in such a way, that the image point of the analyzing magnet formed the object point of the ESA. The angular acceptance of the ESA in horizontal direction is 22.5 mrad, which does not limit the transmission of the analyzer. The vacuum chamber is sealed with Viton and reaches a vacuum below 10^{-7} Torr. The good vacuum is essential to reduce charge changing and scattering of the ions inside the ESA.

If all horizontal slits at the analyzing side are closed to ±2 mm (as we do for heavy ion measurements), we obtain a nominal energy resolution of $E/\Delta E = 1000$. Together with the high momentum resolution of the analyzing magnet, $p/\Delta p = 635$, we have sufficient separation between the isotopes of the heaviest elements. The remaining background stems from charge changing and scattering processes of intense beams that accompany the ions of interest. It can be reduced by additional filters and is distinguished by energy and TOF measurements in the detectors (see Section 5). For the analysis of ^{14}C and ^{26}Al a moveable silicon detector can be inserted at the image position of the ESA (see Fig. 1). The high resolution of the ESA results in very clean energy spectrum for these ions, with virtually no background ions interfering with the radionuclides of interest.

2.5. The heavy-ion beam line system

Since different detectors are used for different ions, a switching magnet was mounted at the end of the ESA exit beam line (see Fig. 1). Straight through the switcher at the 0° exit the ^{10}Be detector system is mounted. The nominal radius of the beam to the +20° exit port, where the heavy ion detector is mounted, is 1.372 m. The ME/q^2 is the same as for the analyzing magnet. A magnetic quadrupole doublet in front of the switching magnet provides focusing at a distance of 1 m behind the magnet. For heavy ions the switching magnet fulfills another important function as an additional stage of background suppression (see Section 5.2).

The heavy ion detector provides both time-of-flight (TOF) and energy signals (Fig. 4). Only the TOF detector has sufficient resolution to distinguish neighboring isotopes. The main function of the energy signal is to discriminate mass/charge ambiguities because they gain different energies in the accelerator due to their different charge state (see Section 5.1).

The TOF signal is derived from the time-of-flight between two similar timing detectors separated by a flight path of 1.5 m. In each timing detector the ions induce secondary electrons at an ultra-thin diamond-like

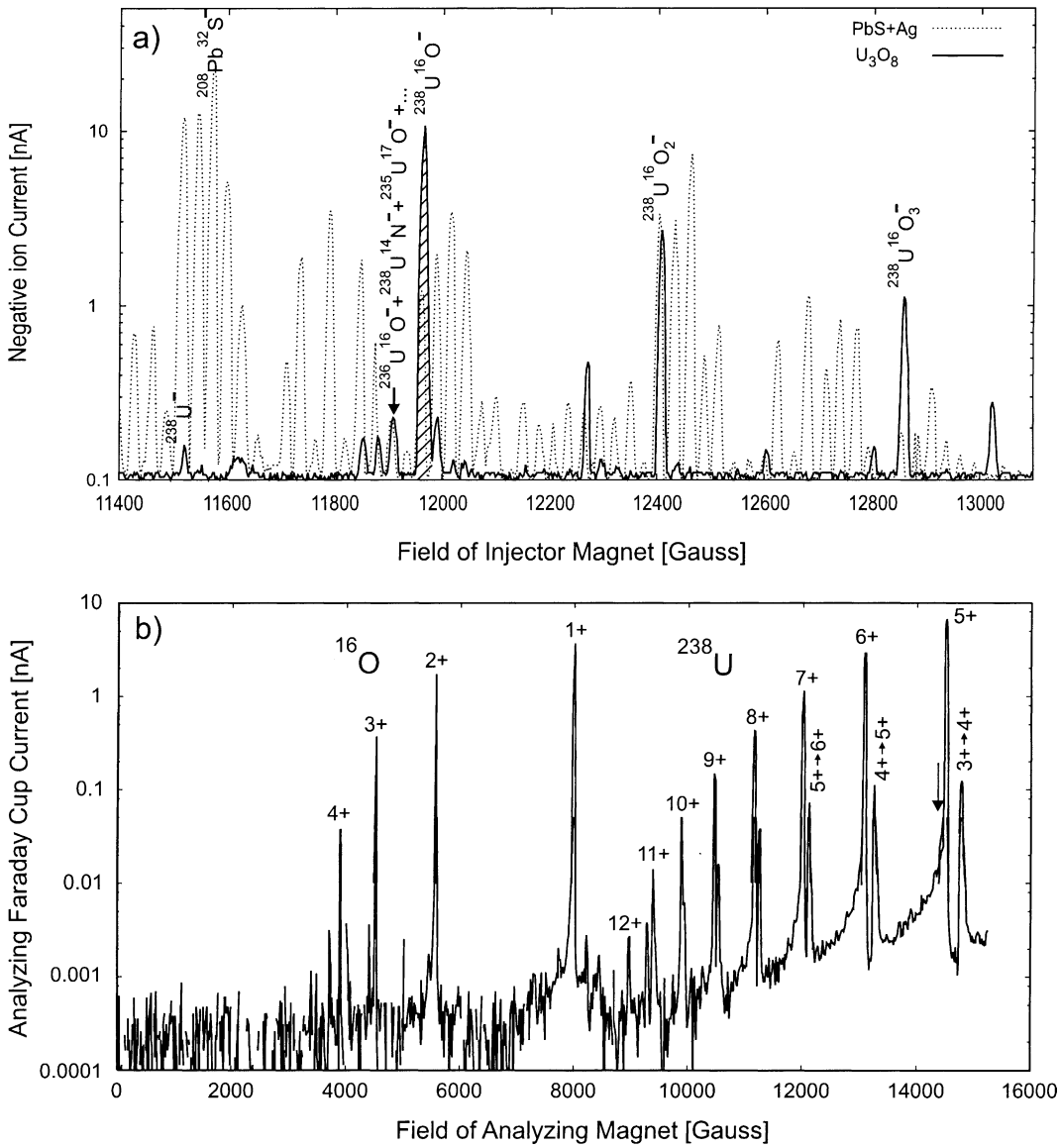

Fig. 3. (a) Injector magnet scan of negative ions from a U_3O_8 target (solid line), and from a PbS + Ag target (dotted line). The rich negative-ion mass spectrum from PbS + Ag is used to calibrate the mass scale. The $^{238}U^{16}O^-$ peak (mass 254) yields the highest current. For the ^{236}U measurement we inject mass 252 ($^{236}U^{16}O^-$). The strongest contribution to the visible peak is probably due to $^{238}U^{14}N^-$ (see Section 5). (b) Analyzing magnet scan for an injected mass of 254 ($^{238}U^{16}O^-$) at 3 MV terminal voltage. The molecules break up into various charge states of ^{16}O and ^{238}U. The origin of the charge-changing tails and the peaks are described in the text. The arrow indicates the position of $^{236}U^{5+}$ relative to the $^{238}U^{5+}$ peak when $^{238}U^{14}N^-$ is injected (see text).

carbon foil (DLC foils); the electrons are reflected by an electrostatic mirror, collected and multiplied by a micro channel plate. The outgoing signal is a very short negative pulse (rise time of less than 1 ns). The start and the stop signals are amplified and fed into a time-to-amplitude converter (TAC). The time resolution (FWHM) of the whole time-of-flight setup is 300–400 ps.

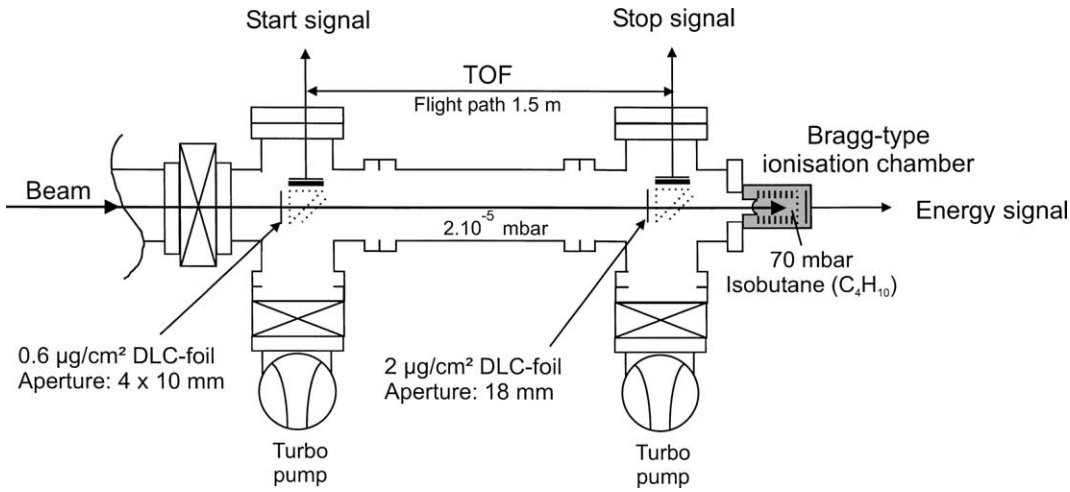

Fig. 4. Schematic setup of the heavy ion detection system. Details of the system are described in Section 2.5.

The DLC foils were produced at the Kurchatov Institute at Moscow by glow-discharge sputtering of graphite inside a low-density krypton plasma [17]. These foils are the thinnest carbon foils available anywhere, and are mounted on an extremely flat Cu mesh (1.2 μm wire thickness) of 90% transmission. For the start detector we used a foil with a thickness of 0.6 μg/cm^2. These foils induce minimal energy loss and almost no angular straggling to the passing ions, verified by a scattering experiment (Fig. 5) and

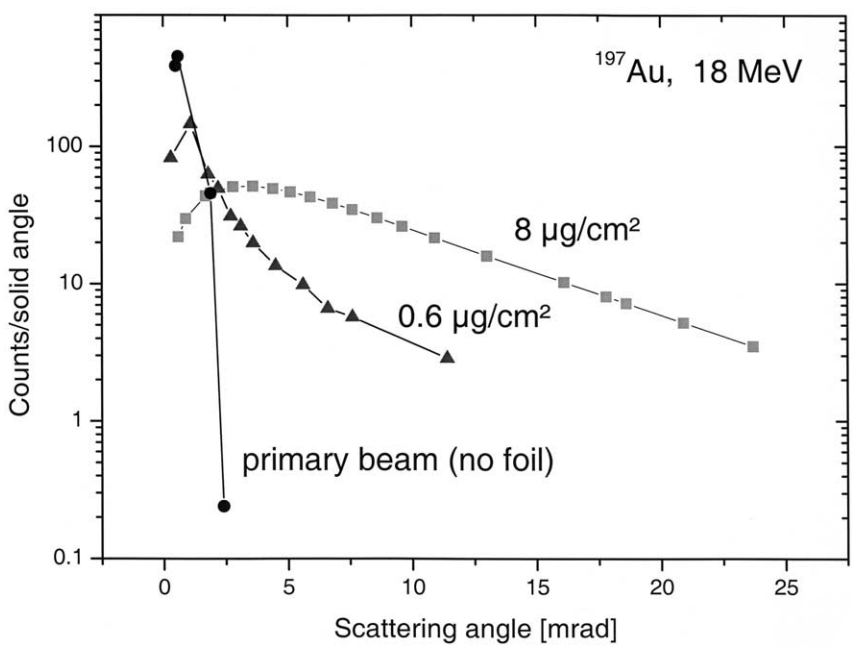

Fig. 5. Angular distribution of 18 MeV ^{197}Au ions scattered from diamond-like carbon (DLC) foils with two different thicknesses. These measurements were performed in a separate scattering experiment with a small-aperture moveable detector. The solid-angle corrected intensity is plotted vs. the scattering angle. For comparison, the primary beam (no foil) is also shown.

phase space measurements (see Section 3). This is a main advantage to minimize the losses of ions due to scattering. In addition, one could increase the flight path to get a better relative time resolution. For example, the ^{238}U ions at 18 MeV need approximately 400 ns for the flight path of 1.5 m. With an overall time resolution (FWHM) of 400 ps we achieve a relative time resolution of 10^{-3}. For the stop detector we use a slightly thicker foil (2–4 μg/cm^2) with a larger aperture of 18 mm. Because of the short distance to the final energy detector angular scattering is not so critical.

The two timing detector have additional three grids, each with a transmission of 95%, to accelerate and bend the electrons from one side of the foil onto the micro channel plates. The optical transmission through both timing detectors is 60%.

For the energy measurement we use a Bragg-type ionization chamber, although a dE/dx determination is not possible at our low heavy ion energies. The ions pass an entrance window (0.5–0.9 μm Mylar) and are finally stopped in a gas volume. As counting gas we use isobutane (C_4H_{10}). Its high density allows stopping the ions inside the active volume at low pressure. An electrical field accelerates the produced charges, which is parallel to the beam direction. This provides better energy resolution because even the electrons produced shortly after the entrance window are collected. The diameter of the entrance window is 16 mm. To avoid increasing the thickness of the entrance window, we used a coarse supporting grid with a transmission of 99%. Measurements showed that a 0.5 μm Mylar foil survives up to 400 mbar with the additional supporting grid, where as it would break at 130 mbar without any support. Our working pressure is about 70 mbar (depending on the ion species and energy). The energy resolution (FWHM) we achieve is 3–5%. This is better than for a surface barrier detector (about 10%), which, in addition, shows a significant pulse height deficiency due to incomplete charge collection. (A first test with a newly developed calorimetric low temperature detector, shows a very promising energy resolution of about 0.5%, and a linearity of the response over a wide energy and mass range [18]). For our purpose the Bragg-type detector is sufficient since it is used to distinguish the energy/charge ambiguities, which are separated by about 20% in energy. Another advantage is the robustness against high count rates. This is usually required for the tuning procedure where we tune the attenuated beam of a stable isotope on count rate in the detector with more than 10^4 counts per second. For actual measurements of rare radioisotopes, we usually have count rates well below 10^3 counts per second.

3. Simulation and experimental analysis of the ion optics

The decisions how to re-arrange the analyzer beam line were based on ion optical calculations. The first-order matrices from [19,20] were implemented in a Mathematica [21] program to simulate the individual ion trajectories. These calculations were supplemented by experimental analysis of the ion optics after each step of the beam line upgrade. For the beam diagnostics a moveable slit and a NEC-type beam profile monitor have been combined to measure the emittance of the ion beam [22]. As the phase space contains the complete information of the beam, this allows extrapolating the profile along the optical axis. By these means, we can check the positions and diameters of the beam waists directly from the plots. The measured divergence α for heavy ion beams (e.g., for $^{197}Au^{5+}$ FWHM(α) = 2.0 mrad after the analyzer magnet) is larger than for light ions (e.g., for $^{13}C^{3+}$ FWHM(α) = 1.1 mrad). We think that the reason lies in the larger angular scattering of the heavier ions in the stripping gas.

4. Measurement procedure

The details of the measurement procedure vary for the different radionuclides. The accuracy of the AMS measurement depends on the reproducibility of the ion optical transmission for different isotopes and

samples. Instabilities in the machine and differences in the sample geometry will induce changes of the beam geometry and consequently of the transmission through every aperture, where parts of the beam are lost. Generally, a reduction of the losses will increase the accuracy of the results [23]. Therefore, the goal of machine tuning is always to maximize the ion optical transmission through the various apertures. Higher efficiency and shorter measuring time are further advantages of this procedure.

We tune the ion-optical components with a pilot beam of a stable or abundant neighboring mass ($^{238}U^{16}O^-$ for instance for ^{236}U). The horizontal slits in front of and after the injector magnet are set to a narrow opening (±1 mm). Nine focusing and steering elements are optimized by maximizing the current in the Faraday cup after the accelerator. This is done fully automated by our program called AUTOMAX [24]. The analyzing side is optimized in a similar way using positive ions (e.g., $^{238}U^{5+}$). Here the horizontal slits are set to ±2 mm. Analyzing magnet, ESA and all focusing and steering elements are optimized by maximizing the current in the last Faraday cup just before the detector. The last magnetic quadrupole doublet and the switching magnet are optimized by maximizing the count rate from the attenuated pilot beam in the energy detector. Once a setup for the pilot beam is found we scale the main components (voltage at the chamber of the injector magnet, accelerator voltage, analyzer ESA) to the mass we want to measure. Systematic investigations showed that if the relative mass difference is sufficiently small, we need not change the lenses and the steerers. We avoid changing magnetic components, which are usually slower and less reproducible.

For normalization, a reference isotope of the same element must be measured together with the wanted radionuclide (e.g., ^{238}U for ^{236}U measurements). Measurement intervals for the reference ion species and the wanted ion species must be alternated. For heavy ions, where we also change the accelerator voltage and in some cases the analyzer ESA, this cannot be achieved with our fast sequencing hardware, which controls only the voltage at the injector magnet chamber and a pair of steerers. So we take resort to slower, software controlled sequencing, where we switch between the reference ion and the radionuclide every 5 min. A Faraday cup is inserted at the image position of the analyzing magnet, if the current of the reference ion (e.g., ^{238}U) is measured. However, the fast sequencing hardware is used to trace output variations from the ion source. During both the measurement of the ion of interest and the reference ion, the voltage at the injector magnet chamber is changed several times per second to deflect the negative ion beam of the reference ion into an offset cup for a short time interval.

5. Background suppression for heavy ion measurement

5.1. Background of lower masses

One main difference to the detection of lighter ions (^{10}Be, ^{14}C, ^{26}Al) is the larger possible number of interfering molecular ions. Although all molecules are destroyed in the stripper, the leakage of fragments through the analyzing system (see Fig. 3) can make a measurement impossible by paralyzing the detector system with too high a counting rate. If the filters are tuned for a certain combination of mass M, charge state q, and energy E, neither magnetic fields nor electrostatic fields nor a combination of both can separate interfering ions which share the same ratios between these basic ion parameters. Unfortunately ions with the same M/q in the analyzer will unavoidably have gained the same E/q during molecular fragmentation, stripping and acceleration [25].

If we look, for instance, at ^{182}Hf with $M = 182$, $q = 4$ and $E_{182} = (E_{inj} + e\,TV)182/277 + 4e\,TV$ we cannot suppress zirconium ions with $M = 91$, $q = 2$ and $E_{91} = (E_{inj} + e\,TV)91/277 + 2e\,TV$, since $182/4 = 91/2$ and $E_{182}/4 = E_{91}/2$. In the final TOF-vs.-energy spectrum of a $^{182}Hf^{4+}$ measurement (Fig. 6) the peak of $^{91}Zr^{2+}$ can be clearly identified.

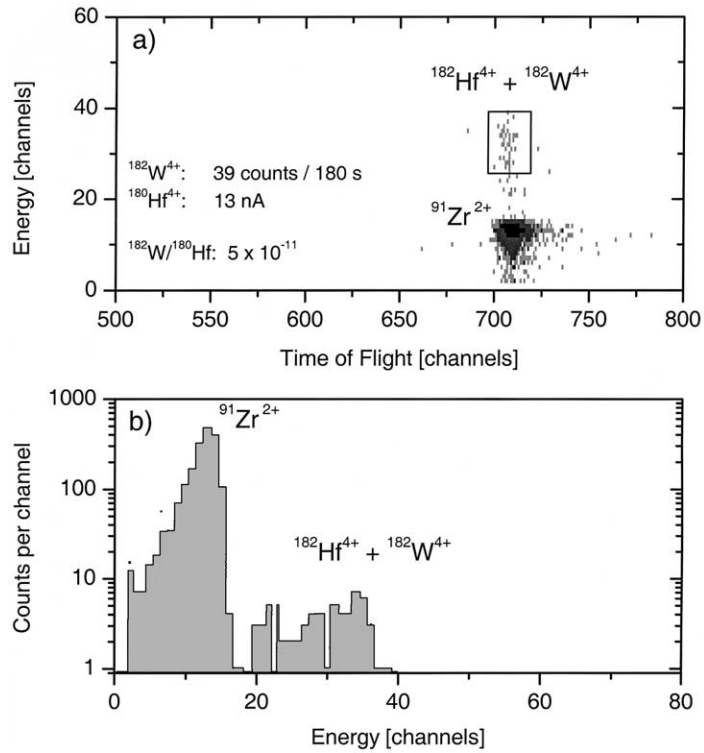

Fig. 6. (a) Time-of-flight (TOF)-vs.-energy (E) spectrum for a measurement to assess the background of ^{182}W for a ^{182}Hf detection with HfF_5^- injection. (b) Projection of (a) onto the energy axis.

When investigating ions of mass M, it is therefore advantageous to work with a charge state q, which shares no common divider n with M. For the heaviest ions, ambiguities with even higher mass, charge state and energy do not exist. Atoms with mass M/n reach the rare isotope detector as ions with charge state q/n and energy E/n, whenever they can form molecular negative isobars in the injector. At low count rates these ambiguities can be distinguished by their different energy with an energy-sensitive detector, but high count rates usually blind such detectors. So for every radionuclide a proper target material, an injected negative ion species and an analyzed charge state must be chosen. Even if mass and charge state have no common dividers, for a different charge state q combinations of mass/charge may exist which show only $1/q$ of the separation of neighboring masses in the same charge state as the wanted ion.

5.2. Background of neighboring masses

It is a general observation in AMS that ion optical filters are passed with a small probability by background ions of neighboring masses even if the expected separation is large. If we exclude ion-optical aberrations, the main reason for this “leakage” can be charge-changing processes along the path of the ions due to residual gas. Angular scattering on the residual gas, on electrodes, slits or vacuum chamber walls can also allow background ions to pass a filter.

The leakage can be reduced by simply adding more filter elements. Every stage provides several orders of magnitude of suppression, until the required background reduction is achieved. Common sense suggests that background ions matching one of the filters (i.e., correct energy over charge state E/q for an ESA, correct momentum over charge state p/q for a magnet,

or correct velocity v for a Wien-filter) can pass with fewer charge changing processes and therefore will be enriched in the residual background. However, cross sections and geometry may alter this general rule, so each type of background requires individual analysis. The goal of the recent VERA upgrade was to reduce this background.

We made systematic investigations with uranium ions. In the original beam line configuration only the analyzing magnet provided suppression of neighboring masses for heavy ions. The separation between $^{236}U^{5+}$ and interfering $^{238}U^{5+}$ after the Wien-filter was only 0.8 mm, which allowed no background reduction. In the TOF-vs.-energy histogram (Fig. 7) we see that the tail of a background peak related to ^{238}U extends into the area where the ^{236}U is expected. The counts in this area correspond to a background in $^{236}U/^{238}U$ of 1×10^{-8}.

The origin for this background was studied by injecting mass 254 ($^{238}U^{16}O^-$) instead of 252 ($^{236}U^{16}O^-$). In the analyzing magnet scan (Fig. 3b) we can see all fragments up to the maximum field strength of 1.53 T. At lower magnetic fields there are the different charge states of oxygen (^{16}O) which have gained different energy in the accelerator. For ^{238}U we see the charge states down to 5+ which is the lowest charge state we can bend with the magnet. Between these peaks, we can see a continuum caused by charge changing processes within the accelerator tubes. Every peak has a tail towards lower energies of ions which have changed from a lower charge state to a higher one, e.g., from 4+ to 5+. They have less energy than the regular 5+ ions, and the energy deficit depends on the position where the charge change took place. The probability is highest close to the gas stripper, where the vacuum is worst. The tail ends in a peak at the magnetic rigidity of ^{238}U ions with the energy of regular 4+ ions, but with charge state 5+. This peak is caused by charge changing from 4+ to 5+ between the accelerator exit and the analyzing magnet entrance, which comprises a relatively long section (∼5 m) of the beam line.

For regular ^{236}U measurements we inject $^{236}U^{16}O^-$ (mass 252). However, these ions are always accompanied by other molecular ions. Typically we measure a current of or below 1 nA in the injector (Fig. 3a), which was found to be mainly $^{238}U^{14}N^-$. The $^{238}U^{14}N^-$ component is probably due to residual nitrogen from the combustion of the uranylnitrate to U_3O_8, which was used as sample material. The molecule breaks up in the stripper, and the resultant $^{238}U^{5+}$ ions will undergo the similar charge changing

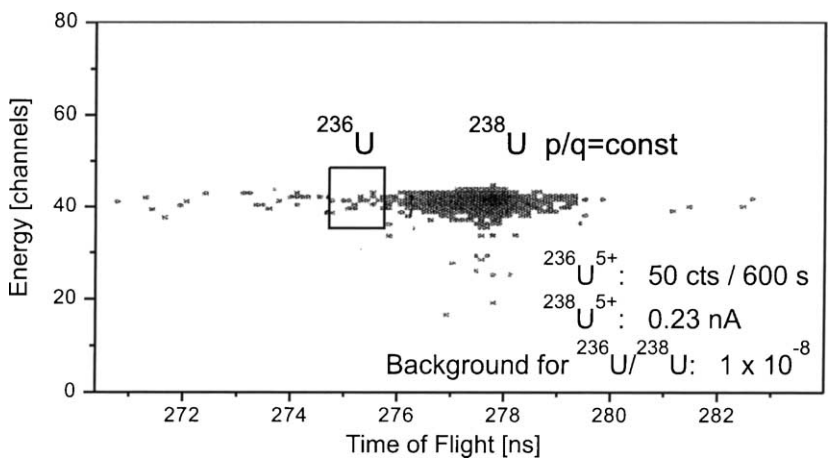

Fig. 7. Time-of-flight (TOF)-vs.-energy (E) spectrum of ^{236}U measured with the original setup (analyzing magnet with Wien-filter). The overwhelming ^{238}U background makes a ^{236}U measurement at natural levels ($^{236}U/^{238}U$ below 10^{-10}) impossible. Different from the description in Fig. 4, the flight path in this measurement was only 972 mm, and the efficiency of detection $^{236}U^{5+}$ ions relative to $^{238}U^{5+}$ was 4%.

processes in the accelerator column as those originating from $^{238}U^{16}O^{-}$ and shown in Fig. 3b. The arrow in this figure indicates the position of ^{236}U in the background continuum, which is used to estimate the suppression of $^{238}U^{5+}$ from $^{238}U^{14}N^{-}$. We see that due to charge exchange in the accelerator column several permil of the $^{238}U^{5+}$ ions can still pass the magnet when it is set for $^{236}U^{5+}$. This background has the same magnetic rigidity p/q as $^{236}U^{5+}$, which implies

$$\Delta E/E = \Delta M/M. \quad (2)$$

These ions have both higher mass and lower energy, and therefore are slower. Using formula (1) we obtain for the relative flight time difference in the TOF detector:

$$\Delta t/t = -\Delta v/v = -\tfrac{1}{2}(\Delta E/E - \Delta M/M) = \Delta M/M \ (p/q = \text{const}). \quad (3)$$

The background peak in Fig. 7 corresponds to this difference in time-of-flight. The large background tail made a measurement of ^{236}U at natural levels impossible with the old setup.

The high resolving power of the ESA (radius $r = 2.0$ m) provides the required suppression. Considering formula (2), the ESA, which is sensitive to E/q only, can further suppress the background with the same magnetic rigidity. The separation at the image slits is $\Delta x = 2r\ \Delta E/E$. In our case $^{238}U^{5+}$ with the same magnetic rigidity as $^{236}U^{5+}$ is separated by 34 mm.

After the ESA, in the TOF-vs.-energy histogram (Fig. 8a) for a natural uranium sample ($^{236}U/^{238}U \sim 6 \times 10^{-11}$), we see mainly ^{236}U. However, the $^{238}U^{5+}$ ions with the same magnetic rigidity as $^{236}U^{5+}$ are not yet completely suppressed. In our understanding, these ^{238}U ions must undergo a second charge change (Fig. 9). To obtain the correct energy to pass the analyzing magnet, the first change from 4+ to 5+ has to take place inside the accelerator column shortly after the terminal (a frequent process, as shown above). The second charge change from 5+ back to 4+ must take place inside the ESA. The charge change causes a change of the bending radius, and there is a certain position near the exit from where the $^{238}U^{5+}$ ions will pass through the image slits. The ions are less than 10 mm off the mean path when the charge change takes place.

In the TOF spectrum (Fig. 8c), between the $^{236}U^{5+}$ and the $^{238}U^{5+}$ with the same magnetic rigidity there are counts with about half the TOF separation. Since we found no ^{237}Np in our sample material, we think that this corresponds to $^{238}U^{5+}$ with the same energy as $^{236}U^{5+}$:

$$\Delta t/t = -\Delta v/v = \tfrac{1}{2}\Delta M/M \quad (E/q = \text{const}) \quad (4)$$

i.e., these ions show the half TOF-separation of ions with constant magnetic rigidity (compare formula (3)). This agrees with the general rule that the ESA will suppress all background ions except those with the same E/q as $^{236}U^{5+}$. However, further systematic investigations are required to understand which charge changing or scattering processes are involved, and where they can take place.

The processes allowing background to pass the high resolving filters involve charge changes. Ions with a wrong charge state can be suppressed even by components of low selectivity. The resulting gain in background suppression can be clearly seen in Fig. 8b. The switching magnet has been added as an additional filter element after the ESA. Since the path inside the switching magnet is short the separation between neighboring uranium isotopes with the same energy is only 2 mm. On the other hand, the residual background before the switching magnet is dominated by ^{238}U ions in charge state 4+ which can be completely suppressed. In Fig. 8d the ^{238}U peak corresponding to the same magnetic rigidity has disappeared. Pleasingly, the background, which we interpreted as $^{238}U^{5+}$ with the same energy as $^{236}U^{5+}$, is also suppressed. Similar background processes are also possible for ^{235}U, and in the TOF-vs.-energy histograms we sometimes observed corresponding counts.

This investigations showed that charge-changing of ^{238}U ions was the main source of background during ^{236}U measurements before adding the switching magnet. However, this is consistent with the expectations from the different cross sections: the scattering cross section is in the order of 10^{-20} cm^2 whereas

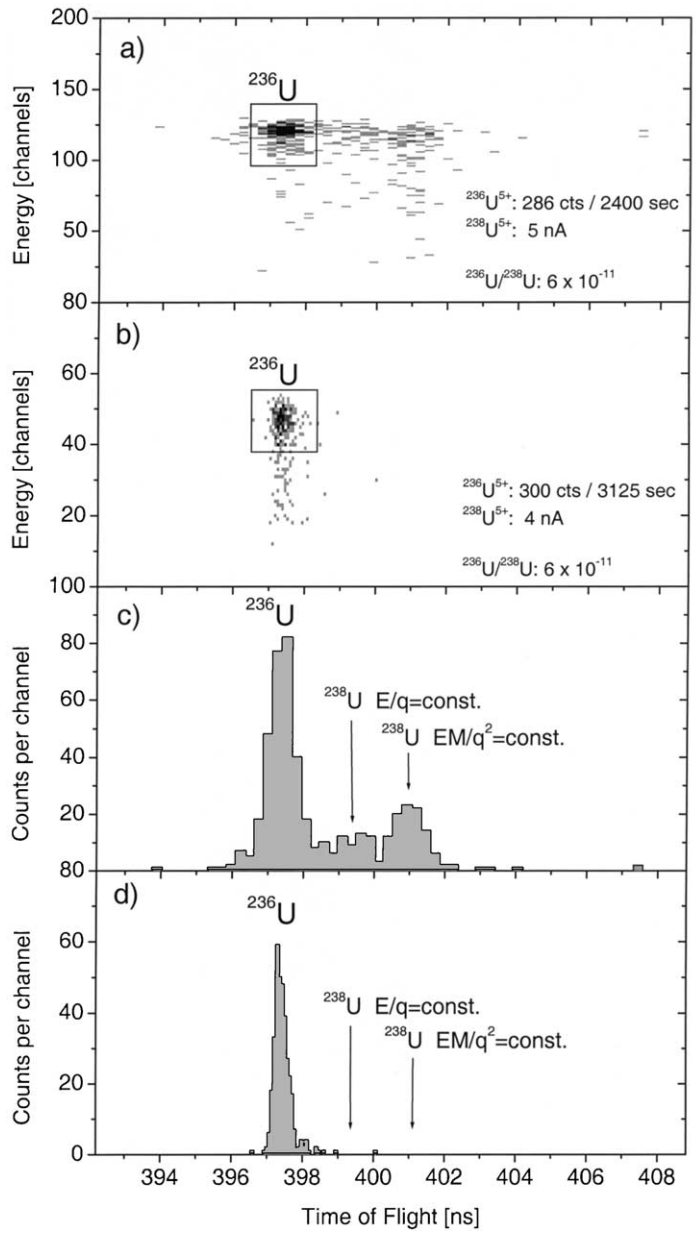

Fig. 8. Comparison of time-of-flight (TOF)-vs.-energy (E) spectra measured at different stages of the VERA upgrade for the detection of ^{236}U (injected as $^{236}U^{16}O^-$ and analyzed as $^{236}U^{5+}$). (a) After replacing the Wien-filter with the ESA. Compared to spectra Fig. 7 and (b), the TOF resolution in this measurement was worse due to a defective amplifier. (b) Compared to (a), an additional analysis of the beam is provided by the 20° bend in the switching magnet. (c) Projection of (a) onto the TOF axis. (d) Projection of (b) onto the TOF axis.

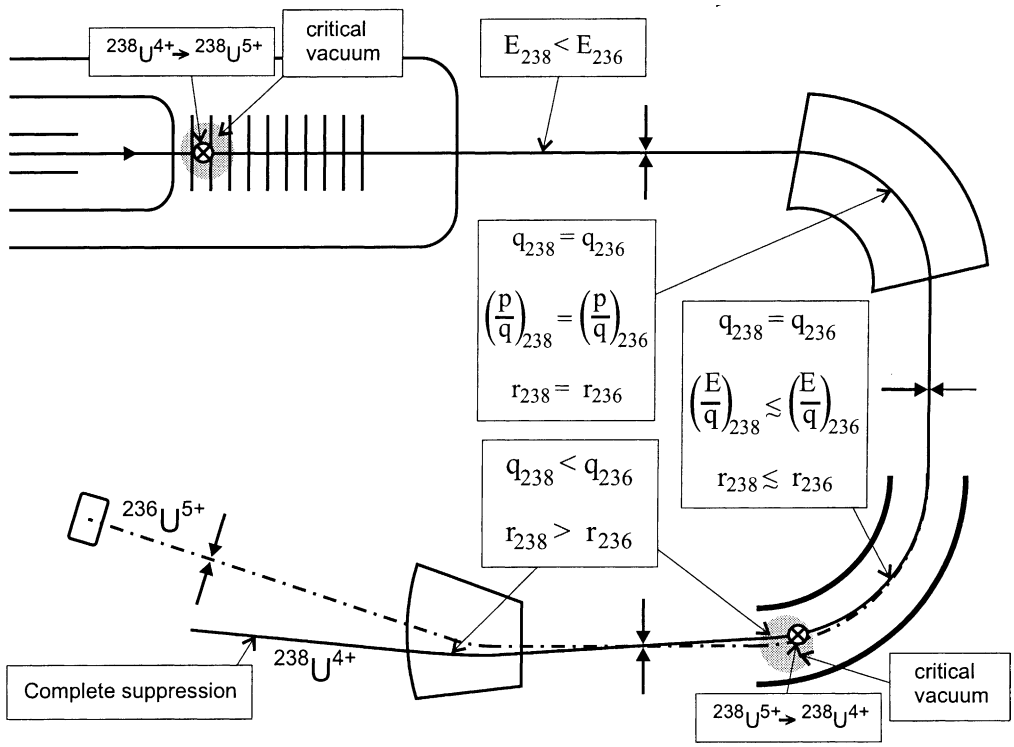

Fig. 9. Schematic presentation of the source of ^{238}U background having the same magnetic rigidity (momentum/charge state ratio) as $^{236}U^{5+}$ ions in the 90° analyzing magnet. The removal of the degeneracy by a charge exchange towards the exit of the ESA and the subsequent separation in the 20° switching magnet is indicated (see Section 5.2).

the cross-section of charge changing is 10^{-16} to 10^{-15} cm^2 [26].

Recently, we have mounted the small Wien-filter from our original setup between the accelerator and the analyzer magnet (see Fig. 1). We did not perform any measurements yet, but a further suppression can be expected if part of the background ions have "wrong" charge states at this position.

6. Measurement possibilities and outlook

If, like in our case, the interfering background is removed, the major remaining limiting factor concerning the sensitivity is the negative-ion sputter yield in the ion source, which is for most heavy ions well below 1%. Stripping yield (3–6%) and detector efficiency (20–30%) are further limitations, but less significant. Clearly, there is still potential for further improvements.

After the upgrade, VERA fulfills the requirements for a universal AMS facility for cases where no stable isobars exist. This, together with the good stability of the comparably small machine and the possibility to measure up to 40 samples in one computer controlled batch makes our AMS system suitable for applications of heavy radionuclides with almost "^{14}C-like" running conditions. Some of the ongoing measurements of heavy ions and their applications are described briefly in the following.

6.1. ^{210}Pb, a comparison with decay counting

^{210}Pb with its short half-life of 22.3 years is not a typically AMS radionuclide. It is usually measured via decay counting with a liquid scintillation detector

[27]. However, at VERA it was used to develop the measuring procedure for heavy ions. Using the original setup in combination with a TOF detector for additional mass discrimination, we were able to demonstrate the measurement of ^{210}Pb down to isotope ratios of $^{210}Pb/^{208}Pb = 3 \times 10^{-11}$ [28]. This was only possible at this stage with the use of PbF_3^- ions, to avoid a simultaneous injection of the other Pb isotopes. The negative ion mass spectrum of the PbF_2 material (Fig. 2) demonstrates the high mass resolution achieved with the new injector slits. The overall sensitivity achieved for the ^{210}Pb detection (10^{-5} of the total amount of ^{210}Pb could be detected) is comparable to the conventional decay counting.

6.2. ^{236}U, a neutron flux monitor

^{236}U with a half-life of 23.4 million years is one of the heaviest radionuclides of interest for AMS. It was first detected in a uranium ore by the Toronto AMS group [9]. ^{236}U is produced in nature from ^{235}U by neutron capture. The isotopic ratio $^{236}U/^{238}U$ depends strongly on the thermal neutron flux in the material. This makes the radioisotope very suitable as a neutron monitor. In contrast to spent nuclear fuel with $^{236}U/^{238}U$ isotope ratios in the order of 10^{-3}, in natural samples isotope ratios are expected to be in the range of 10^{-10} to 10^{-14}. Up to now detection limits of 3.6×10^{-10} [29], 6×10^{-10} [30], $\sim 1 \times 10^{-11}$ [31] and 1×10^{-12} [44] were reached at other facilities. The reached sensitivity was not limited by counting statistics, but by background from other nuclides.

For our first measurements we used aliquots from uranylnitrate $UO_2(NO_3)_2 \cdot 6H_2O$, which had been stored in sealed bottles for decades in the basement of the Institute for Isotope Research and Nuclear Physics in Vienna [32]. The bottles have labels which read “K. k. Uranfabrik Joachimsthal”, and originate from the famous uranium mines which supplied material to Pierre and Marie Curie at the turn of the 19th century.

For the measurement we used U_3O_8 as target material and extracted up to 100 nA of $^{238}U^{16}O^-$. We used U^{5+} ions at the analyzer, and we measured for ^{238}U a stripping yield of $^{238}U^{5+}/^{238}U^{16}O^- = 0.03$ with the lowest possible stripper gas pressure. Recent investigations showed that using oxygen as stripper gas, a stripping yield of 0.06 can be achieved. The detector efficiency was measured using the $^{235}U/^{238}U$ ratio of the attenuated beam (^{235}U measured as counts in the heavy ion detector and ^{238}U measured as a current in the Faraday cup). The reached efficiency is 30%, which is significantly less than the expected 60%. The reason is yet unknown and need further systematic investigations. With the detector system after the ESA, we have demonstrated by a dilution series a precision of ∼5% for relative measurements of $^{236}U/^{238}U$ at natural levels [32]. However, since a standard material at these levels is not yet established, our absolute result of $(6.1 \pm 0.4) \times 10^{-11}$ for the “K. k. Uranfabrik Joachimsthal” uranium can only be preliminary.

So far, available uranium samples stem from uranium ores, where the neutron fluxes are expected to be high and to produce considerable amounts of ^{236}U. Although Fig. 8b suggests that we can measure isotopic ratios much lower than 10^{-11}, this remains only speculation until we can measure a real blank material containing no ^{236}U. As a next step we plan to measure uranium collected from water samples, where we expect a much lower ^{236}U concentration. At low isotopic ratios the measuring time may become a limitation. To reach an isotopic ratio of 10^{-14} (which is expected for uranium embedded in rock at a level of 1 ppm), we will collect one count every 8000 s assuming a (realistic) $^{238}U^{5+}$ current of 10 nA. Fortunately, the uranium targets give currents for many hours.

6.3. ^{244}Pu, a possible supernova remnant

^{244}Pu has the longest half-life (81 million years) of all plutonium isotopes. It can only be produced at high neutron fluxes in supernovae or in nuclear bombs.

First measurements of targets containing trace amounts of plutonium show promising results. Similar to the uranium measurements we injected PuO^- and analyzed Pu^{5+}. Since there are only a few Pu atoms (several 10^7 to 10^8) in the sample material (mainly iron oxide), the system was tuned with ^{238}U and the setup scaled to the various plutonium isotopes. As

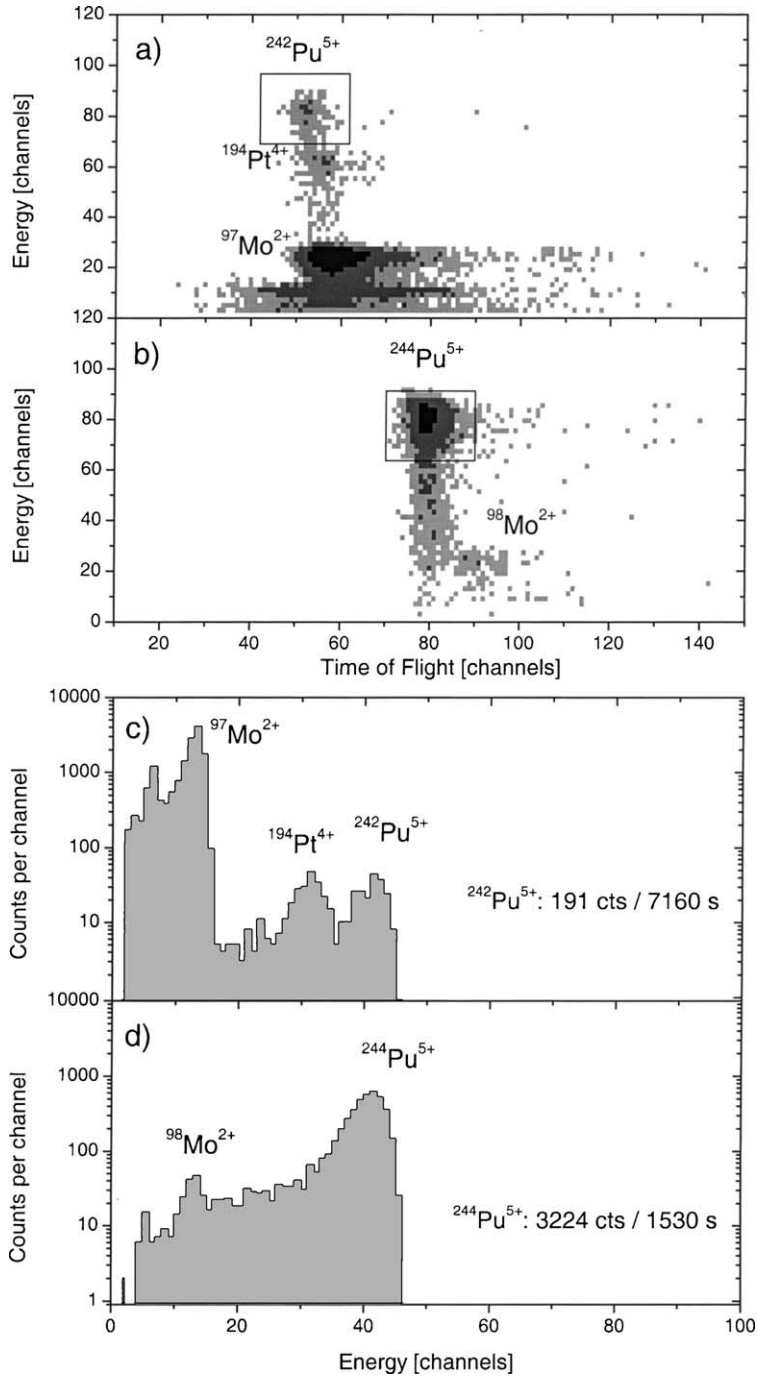

Fig. 10. TOF-vs.-energy spectra measured for a ^{244}Pu calibration sample. The ^{242}Pu/^{244}Pu isotope ratio in this sample was determined from α-activity to be 0.0112. An aliquot containing $\sim 2 \times 10^7$ ^{242}Pu atoms (corresponding to only $\sim$1 α-decay in 10 days) was measured with AMS, resulting in a ^{242}Pu/^{244}Pu isotope ratio of 0.0127 ± 0.0008. (a) ^{242}Pu spectrum injected as $^{242}Pu^{16}O^-$ and analyzed as $^{242}Pu^{5+}$. (b) ^{244}Pu spectrum injected as $^{244}Pu^{16}O^-$ and analyzed as $^{244}Pu^{5+}$; (c) and (d) are the projections of (a) and (b), respectively, on the energy axis. The molybdenum background ions match the mass/charge state ratios of the respective plutonium isotopes, and are therefore the most likely explanation for the background. The $^{194}Pt^{4+}$ background was positively identified by using a platinum target in the ion source.

reference ion we used ^{242}Pu, which was also counted in the detector. We measured the ^{242}Pu/^{244}Pu ratio in a ^{244}Pu standard prepared at Argonne National Laboratory. The isotopic ratio of ^{242}Pu/^{244}Pu determined from α-activity is 0.0112, and this value could be reproduced by our measurement in a sample diluted to contain only $\sim 2 \times 10^7$ atoms of ^{242}Pu. The ^{242}Pu and ^{244}Pu spectra are shown in Fig. 10. A total of 191 ^{242}Pu atoms were detected (Fig. 10a). Since only part of the sample was sputtered, we obtain a lower limit of the overall efficiency (counts/atoms in sample) of $\sim 10^{-5}$. With an assumed negative ion yield of 0.3% [33], a measured 5+ stripping yield of 3% and a detection efficiency of 30%, we calculate 2.7×10^{-5}. This agrees well with the measured efficiency, and is considerably higher than the efficiency of $\sim 3 \times 10^{-6}$ reported recently for Pu AMS measurements at a large tandem accelerator [34].

For planned measurements of natural ^{244}Pu the highest possible sensitivity is needed for the detection of a few ^{244}Pu atoms in a sample. In that case it is especially important to understand the possible sources of background. One application of ^{244}Pu is the search for a recent (within the last several 100 million years) supernova, which may have produced enough ^{244}Pu to leave a detectable signal in slowly accumulating reservoirs such as deep-sea sediments [34]. A possible first evidence for the shorter-lived supernova product ^{60}Fe ($t_{1/2} = 1.5 \times 10^6$ a) was reported by the Munich AMS group [35].

6.4. ^{182}Hf, an extinct radionuclide

^{182}Hf is a long-lived radionuclide which has not yet been exploited by AMS. We are currently investigating the conditions to measure it with our new heavy ion analysis system. In contrast to the radionuclides mentioned above, the main problem of the detection of ^{182}Hf is the interfering stable isobar ^{182}W, which pass all ion-optical filters together with ^{182}Hf and cannot be discriminated in the detector at our low energies. We must reduce the W in the ion source. Therefore, we use HfF_4 mixed with silver powder as target material and $^{182}HfF_5^-$ as injected ion, because ^{182}W forms much less $^{182}HfF_5^-$ ions. The analyzed ion is $^{182}Hf^{4+}$. The reference isotope is ^{180}Hf, the heaviest and most abundant of the 5 stable isotopes. The sensitivity is limited by the remaining ^{182}W. Since ^{182}W has the same mass and energy as the ^{182}Hf it appears at the same position in the TOF-vs.-energy spectrum (Fig. 6). A first detection limit of ^{182}W/^{180}Hf in the order 10^{-10} was achieved with HfF_5^- ions, whereas a ratio of ^{182}W/^{180}Hf $\sim 10^{-4}$ was measured with atomic negative ions.

This nuclide is of interest for the early history of the earth, in particular with respect to the origin of the moon [36]. This early time period of the earth can be investigated through the isotopic anomaly of stable ^{182}W, caused by the in situ decay of now extinct ^{182}Hf [37,38]. However, the half-life of ^{182}Hf is still poorly known, $t_{1/2} = (9 \pm 2) \times 10^6$ a [39]. We plan to re-measure it with greater accuracy by a specific activity measurement combining AMS with a γ-activity measurement. This will either be attempted with material from Hf control rods of a recently retired nuclear reactor, or by using material left over from a high-flux neutron irradiation of Hf, which led to the discovery of the 30-year isomer in ^{178}Hf [40]. In the latter case, the ^{182}Hf/Hf ratio may actually be high enough to measure the isotope ratio by multi collector inductively coupled plasma mass spectrometry (MC-ICP-MS). A similar measurement was performed for a half-life measurement of the long-lived fission product ^{126}Sn [41–43].

Depending on the sensitivity of ^{182}Hf detection we can reach with our new AMS system, a search for live ^{182}Hf as a supernova remnant—similar to ^{244}Pu—in appropriate archives on earth is planned.

7. Conclusion

The current work describes the extension of an AMS system based on a small tandem accelerator to a universal AMS system for all isotopes. Although over 90% of all AMS measurements world-wide are still performed for ^{14}C analyses, other radionuclides are gaining ground. In particular, the heaviest radionuclides are attractive for small AMS facilities because

of the absence of stable isobar interference. The continuing computerization and automatization of these AMS facilities has greatly improved the control of complicated experimental setups. Together with new particle detector systems on the horizon (e.g., cryo-detectors), a bright future for these "non-routine" radionuclides lies ahead.

Acknowledgements

We thank Karl Irlweck and Gabriele Wallner from the Institute of Inorganic Chemistry, University of Vienna, for help in sample preparation. We gratefully acknowledge the supply of several components of the heavy ion detection system by Walter Assmann and Gunther Löbner from the Ludwig Maximilian University Munich. We also thank Martin Suter from the PSI/ETH AMS facility in Zurich and an unknown reviewer for critical comments on the manuscript. This work was supported in part by the U.S. Department of Energy, Nuclear Science Division, Contract no. W-31-109-ENG-38. The authors are indebted for the use of ^{244}Pu sample to the Office of Basic Energy Sciences, U.S. Department of Energy, through the transplutonium element production facilities at Oak Ridge National Laboratory.

References

[1] A.E. Litherland, Ann. Rev. Nucl. Part. Sci. 30 (1989) 437.
[2] D. Elmore, F.M. Phillips, Science 236 (1987) 543.
[3] C. Tuniz, J.R. Bird, D. Fink, G.F. Herzog, Accelerator Mass Spectrometry: Ultrasensitive Analysis for Global Science, CRC Press, Boca Raton, 1998, p. 371.
[4] W. Kutschera, Am. Inst. Phys. Conf. Ser. 495 (1999) 407.
[5] W. Henning, W.A. Bell, P.J. Billquist, B.G. Glagola, W. Kutschera, Z. Liu, H.F. Lucas, M. Paul, K.E. Rehm, J.L. Yntema, Science 236 (1987) 725.
[6] D. Fink, J. Klein, R. Middleton, Nucl. Instr. Meth. B 52 (1990) 572.
[7] K.H. Purser, R.B. Liebert, A.E. Litherland, R.P. Beukens, H.E. Gove, C.L. Bennet, H.R. Clover, W.E. Sondheim, Revue de Physique Appliquée 12 (1977) 489.
[8] G.M. Raisbeck, F. Yiou, A. Peghaire, J. Guillot, J. Uzureau, in: Proceedings of the Symposium on Accelerator Mass Spectrometry, Argonne National Lab Report ANL/PHY-81-1, 1981, p. 426.
[9] X.-L. Zhao, M.-J. Nadeau, L.R. Kilius, A.E. Litherland, Nucl. Instr. Meth. B 92 (1994) 249.
[10] L.K. Fifield, A.P. Clacher, K. Morris, S.J. King, R.G. Cresswell, J.P. Day, F.R. Livens, Nucl. Instr. Meth. B 123 (1997) 400.
[11] W. Kutschera, P. Collon, H. Friedmann, R. Golser, P. Hille, A. Priller, W. Rom, P. Steier, S. Tagesen, A. Wallner, E. Wild, G. Winkler, Nucl. Instr. Meth. B 123 (1997) 47.
[12] J.A. Ferry, Nucl. Instr. Meth. A 328 (1993) 28.
[13] A.E. Litherland, Nucl. Instr. Meth. B 5 (1984) 100.
[14] A. Priller, T. Brandl, R. Golser, W. Kutschera, S. Puchegger, W. Rom, P. Steier, C. Vockenhuber, A. Wallner, E. Wild, Nucl. Instr. Meth. B 172 (2000) 100.
[15] A. Priller, R. Golser, P. Hille, W. Kutschera, W. Rom, P. Steier, A. Wallner, E. Wild, Nucl. Instr. Meth. B 123 (1997) 193.
[16] http://www.pelletron.com.
[17] V.K. Liechtenstein, T.M. Ivkova, E.D. Olshanski, A.M. Baranov, R. Repnow, R. Hellborg, R.A. Weller, H.L. Wirth, Nucl. Instr. Meth. A 438 (1999) 79.
[18] S. Kraft, A. Bleile, P. Egelhof, R. Golser, O. Kisselev, W. Kutschera, V. Liechtenstein, H.J. Meier, A. Priller, A. Shrivastava, P. Steier, C. Vockenhuber, M. Weber, in: F.S. Porter et al. (Eds.), *Low Temperature Detectors*, Am. Inst. Phys. Conf. Ser. CP605, 2002, p. 405.
[19] H. Wollnik, Electrostatic prisms, in: A. Septier (Ed.), Focusing of Charged Particles II, Academic Press, New York, 1967, p. 163.
[20] H.A. Enge, Deflecting magnets, in: A. Septier (Ed.), Focusing of Charged Particles II, Academic Press, New York, 1967, p. 203.
[21] http://www.wolfram.com.
[22] S. Winkler, R. Golser, W. Kutschera, A. Priller, P. Steier, C. Vockenhuber, in: 35th Symposium of the North Eastern Accelerator Personnel (SNEAP-35), Lund, Sweden, 22–25 October 2001, in press.
[23] W. Rom, R. Golser, W. Kutschera, A. Priller, P. Steier, E. Wild, Radiocarbon 40 (1/2) (1998) 255.
[24] P. Steier, S. Puchegger, R. Golser, W. Kutschera, A. Priller, W. Rom, A. Wallner, E. Wild, Nucl. Instr. Meth. B 161–163 (2000) 250.
[25] L.R. Kilius, X.-L. Zhao, A.E. Litherland, K.H. Purser, Nucl. Instr. Meth. B 123 (1997) 10.
[26] H.-D. Betz, Rev. Mod. Phys. 44 (1972) 465.
[27] G. Wallner, Appl. Radiat. Isot. 48 (1997) 511.
[28] R. Golser, G. Federmann, W. Kutschera, A. Priller, P. Steier, C. Vockenhuber, in: J.L. Duggan, I.L. Morgan (Eds.), Proceedings of the 16th International Conference on the Application of Accelerators in Research and Industry, Am. Inst. Phys. Conf. Ser. CP576, 2001, p. 627.
[29] X.L. Zhao, L.R. Kilius, A.E. Litherland, T. Beasley, Nucl. Instr. Meth. B 126 (1997) 297.
[30] S. Richter, A Alonso, W. De Bolle, R. Wellum, P.D.P. Taylor, Int. J. Mass Spectrom. Ion Process. 193 (1999) 9.
[31] D. Berkovits, H. Feldstein, S. Ghelberg, A. Hershkowitz, E. Navon, M. Paul, Nucl. Instr. Meth. B 172 (2000) 372.

[32] P. Steier, R. Golser, W. Kutschera, A. Priller, A. Valenta, C. Vockenhuber, Nucl. Instr. Meth. B 188 (2002) 283.
[33] L.K. Fifield, R.G. Cresswell, M.L. di Tada, T.R. Ophel, J.P. Day, A.P. Clacher, S.J. King, N.D. Priest, Nucl. Instr. Meth. B 117 (1996) 295.
[34] M. Paul, A. Valenta, I. Ahmad, D. Berkovits, C. Bordeanu, S. Ghelberg, Y. Hashimoto, A. Hershkowitz, S. Jiang, T. Nakanishi, K. Sakamoto, Astrophys. J. 558 (2001) L133.
[35] K. Knie, G. Korschinek, T. Faestermann, C. Wallner, J. Scholten, W. Hillebrandt, Phys. Rev. Lett. 83 (1999) 18.
[36] A.N. Halliday, Earth Planet Sci. Lett. 176 (2000) 11.
[37] C.L. Harper Jr, S.B. Jacobsen, Geochim. Cosmochim. Acta 60 (1996) 1131.
[38] A.N. Halliday, D.-C. Lee, Geochim, Cosmochim. Acta 63 (1999) 4157.
[39] J. Wing, B.A. Schwartz, J.R. Huizenga, Phys. Rev. 123 (1961) 1354.
[40] R.G. Helmer, C.W. Reich, Nucl. Phys. A211 (1973) 1.
[41] P. Gartenmann, R. Golser, P. Haas, W. Kutschera, M. Suter, H.-A. Synal, M.J.M. Wagner, E. Wild, Nucl. Instr. Meth. B 114 (1996) 125.
[42] P. Haas, P. Gartenmann, R. Golser, W. Kutschera, M. Suter, H.-A. Synal, M.J.M. Wagner, E. Wild, G. Winkler, Nucl. Instr. Meth. B 114 (1996) 131.
[43] F. Oberli, P. Gartenmann, M. Meier, W. Kutschera, M. Suter, G. Winkler, Int. J. Mass Spectrom. Ion Process. 184 (1999) 145.
[44] M. Paul, D. Berkovits, I. Ahmad, F. Borasi, J. Caggiano, C.N. Davids, J.P. Greene, B. Harss, A. Heinz, D.J. Henderson, W. Henning, C.L. Jiang, R.C. Pardo, K.E. Rehm, R. Rejoub, D. Seweryniak, A. Sonzogni, J. Uusitalo, R. Vondrasek, Nucl. Inst. Meth. B 170 (2000) 688.